Alfvén Eigenmodes in Shear Reversed Plasmas

B.N. Breizman 1), H.L. Berk 1), M.S. Pekker 1), S.E.Sharapov 2), N.C. Hawkes 2), D.N. Borba 3), S.D. Pinches 4), and JET-EFDA Contributors 5)

1) Institute for Fusion Studies, The University of Texas, Austin, Texas, 78712 USA
2) Euratom/UKAEA Fusion Association, Culham Science Center, Abingdon, Oxfordshire OX14 3DB, UK
3) EFDA-JET Close Support Unit & Euratom/IST Association, Lisbon, Portugal
4) Max-Planck Institut für Plasmaphysik, Euratom Association, Garching, Germany
5) See Annex1 in IAEA 2002 J.Pamela OV-1/1.4

e-mail contact of main author: breizman@mail.utexas.edu

Abstract. Experiments on JT-60U and JET have shown that plasma configurations with shear reversal are prone to the excitation of unusual Alfvén eigenmodes by energetic particles. These modes emerge outside the TAE frequency gap, where one might expect them to be strongly damped. The modes often appear in bunches and they exhibit a quasi-periodic pattern of predominantly upward frequency sweeping (Alfvén Cascades) as the safety factor q changes in time. This work presents a theory that explains the key features of the observed unusual modes including their connection to TAE's as well as the modifications of TAE's themselves near the shear reversal point. The developed theory has been incorporated into a reduced numerical model and verified with full geometry codes. JET experimental data on Alfvén spectroscopy have been simulated to infer the mode numbers and the evolution of q_{min} in the discharge. This analysis confirms the values of q that characterize the internal transport barrier triggering in reversed shear plasmas.

1. Introduction

There are two main reasons why Alfvén eigenmodes are of interest in magnetic fusion research. The first is the concern that these modes can degrade energetic ion confinement [1], particularly the confinement of fusion-produced alpha particles in burning plasma experiments [2]. The second is the observation that benign Alfvén eigenmodes can provide unique diagnostic opportunities via so-called MHD-spectroscopy [3]. Furthermore, there is an impressive amount of high-quality and still not totally explained experimental data from various machines (JET, TFTR, JT-60U, DIII-D, and others) that necessitates a detailed theoretical analysis of the Alfvén modes themselves and of their interactions with the energetic ion population.

The shear Alfvén wave frequency range has been extensively explored in the experiments, with a particularly strong interest in Toroidicity Induced Alfvén Eigenmodes (TAE) [4]. The TAEs are associated with the gaps in the Alfvén continuum, which essentially eliminates the continuum damping effect for these modes. Another way to reduce the role of continuum damping is to place the modes at radial locations with the least spatial dependence in the local shear Alfvén wave frequency

$$\omega_A = \frac{V_A(r)}{R}\left(n - \frac{m}{q(r)}\right) \qquad (1)$$

Here, n and m are the toroidal and the poloidal mode numbers, V_A is the Alfvén velocity, R is the major radius, and q is the safety factor. The frequencies of primary interest for many experiments are roughly of the order of $V_A/(2qR)$, and the mode numbers are often large. It is apparent from Eq. (1) that such modes are more sensitive to the safety factor profile than they

are to the plasma density profile. Any location where *q* is nearly flat should then be viewed as a potential site for the mode. A good example of such a case is the Global Alfvén Eigenmode (GAE) [5,6].

This idea of identifying flat *q* (zero shear) sites concurs with numerous observations of so-called Alfvén Cascades (AC) in tokamak discharges with non-monotonic *q*-profiles. The cascades were discovered on JT-60U [7] and then also found on JET [8, 9] where they have been studied extensively. The cascade modes typically appear in "bunches". They emerge outside the TAE gap and exhibit a quasi-periodic pattern of frequency sweeping, as shown in FIG. 1. It has been revealed that the mode frequencies actually trace the temporal evolution of $\square_A$ due to the time dependence of the safety factor at the zero shear point. However, the experiments exhibit only a subset of the frequencies described by Eq. (1). In particular, most of the observed frequencies move upward when the safety factor decreases in time. This feature indicates that some of the candidate frequencies given by Eq. (1) may not be suitable for establishing an eigenmode. A related issue is that the allowed modes cannot be simply interpreted as conventional GAE's since the latter would have an opposite direction of frequency sweeping [10].

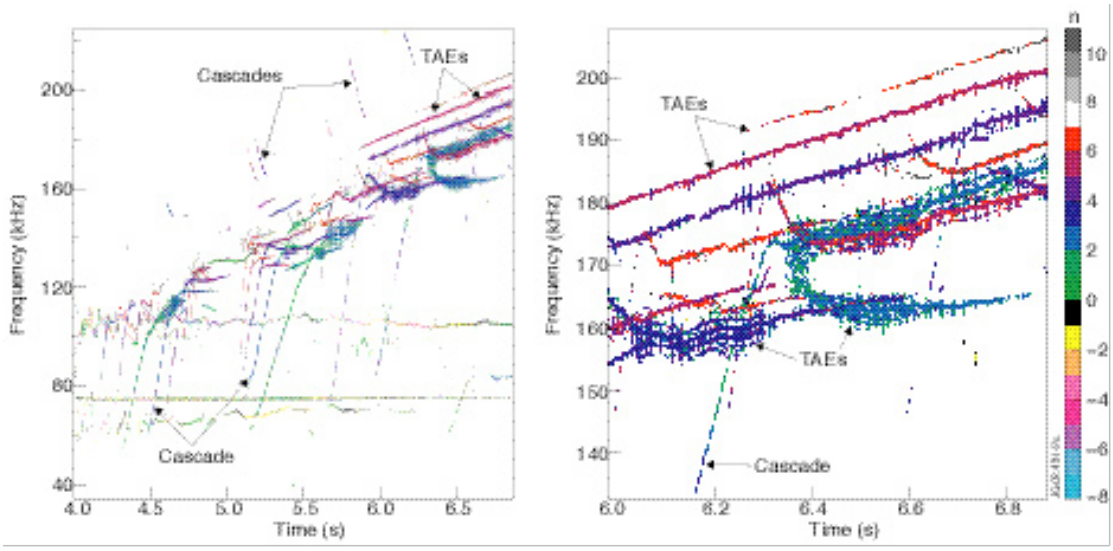

FIG. 1. Alfvén Cascades of sweeping-up and of sweeping-down types, observed in a JET discharge simultaneously with TAEs. The right part of the figure is a zoom of the left part. It shows TAEs, some of which arise from the AC.

In order to establish the "rules" for the mode existence, one has to look specifically at the physics mechanisms that maintain the eigenmode structure. It is essential that there is a degeneracy in the shear Alfvén waves in a plasma that is cold and spatially uniform. In such a plasma, any radial mode structure is compatible with the eigenfrequency determined by Eq. (1). The reason why the mode structure is not robust in this case is that different flux surfaces don't communicate via shear Alfvén signals. Two ways for them to communicate are via radial excursions of particle orbits (including gyro-orbits) and via toroidal MHD-effects. The first option (discussed in Sec. 2 below) was recently examined in Ref. 10 as a primary candidate for the interpretation of Alfvén Cascades below the TAE gap in a plasma with a significant population of energetic particles. The second option is known to give rise to TAE's via coupling of neighboring poloidal harmonics. In Sec. 3, we examine this coupling for the reversed shear case.

2. Energetic Particle Modes

Alfvén Cascades require an essentially non-perturbative fast particle response. This means that the fast particle contribution to the MHD equations affects the very existence of the mode rather than just the mode growth rate. Technically, there is an important simplification in the theory, which applies to deeply reversed shear discharges, including relevant JET discharges. The time-scale of the fast particle ∇B-drift across the mode structure is typically shorter than the bounce period or the mode period $2\pi/\omega$. As a result, most of the energetic particles do not resonate with the mode, and their orbit width is typically larger than the mode width. These features lead to a mode structure that is insensitive to the details of the particle distribution function. They also lead to a spatially local response of the non-resonant particles. In this case, the non-local part of the response is parametrically smaller, which indicates that the mode growth/damping rate is small compared to the real contribution from the energetic particles to the mode frequency. It has been shown in Ref. [10] that the following criterion needs to be satisfied for the energetic particles to establish a cascade mode:

$$Q = -\frac{4\pi eRq_0^2}{cBr_0 q_0''}\frac{d}{dr}\frac{V_A|m-nq_0|}{(m-nq_0)}\left\langle n_h\right\rangle + \left\langle \frac{1}{e} j_{\parallel h}\right\rangle_{r=r_0} > \frac{1}{4} \qquad (2)$$

Here, B is the toroidal magnetic field, n_h and $j_{\parallel h}$ are the fast particle density and parallel current respectively, q_0'' is the second radial derivative of the safety factor, the subscript "0" refers to the zero shear point and the angular brackets denote flux surface averaging. It is noteworthy that the absolute value of Q is independent of m and n, which seems to be the reason why Alfvén Cascades usually consist of many modes.

It follows from the eigenmode equation of Ref. [10] that there is formally an infinite number of radial modes for Q>1/4 but their radial scale length Δr is exponentially small when Q is close to the critical value of 1/4. It is natural to expect these short-wavelength modes to be suppressed since their frequencies are extremely close to the Alfvén continuum. In contrast, for large values of Q (Q>>1), we find that Δr scales as $\Delta r \propto Q^{1/4} r_0 / m$, so that the mode width can even exceed the poloidal wavelength. The lowest radial modes are likely to be the least affected by damping, which makes them relevant candidates to match the experimental data.

Depending on whether q_0 is larger or smaller than m/n, we need either positive or negative gradient of the fast particle density to satisfy Eq. (2). However, only the negative gradient is compatible with the preferred upward direction of frequency sweeping in FIG. 1.

Once the existence of a mode is established, the mode growth rate, associated with resonant energetic particles, can be calculated with the use of perturbation theory. The damping rates due to background plasma can be accounted for in a similar way. Also, the mode saturation level in a weakly nonlinear regime can be calculated straightforwardly with the technique described in Ref. [11].

3. Toroidal Effects and Zero Shear TAEs

The role of toroidicity-induced coupling becomes crucial when the frequency of the cascade mode approaches the TAE gap. However, the conventional analytic description of TAEs does not cover the shear reversal case, which points out the need to modify the theory in order to

accurately connect the cascade modes to TAEs. One particular aspect of this problem is the existence of many TAEs in a single gap in the weak shear limit [12]. In addition, we find that the weak shear case makes it possible for the (second-order) toroidal effects to establish a nearly cylindrical eigenmode with a single dominant poloidal component. Such modes can exist outside the TAE gap and they are basically similar to the energetic particle modes described in Ref. 10, except for the physics mechanism of communication between the flux surfaces.

The conventional TAE modes are known to be associated with "special" values of q [$q = q_{TAE} = (2m \pm 1)/2n$] that represent strongest linear coupling between the m-th and $(m-1)$-th poloidal harmonics. Motivated by the experiments, we assume that the q- profile has a minimum at $q(r) = q_0$ within the plasma cross-section and that q_0 decreases in time. In its motion, the lowest point in the q- profile can go from above to below q_{TAE}. One might argue that there should be no TAE mode until q_0 reaches q_{TAE} and that there should be two modes when q_0 is below q_{TAE}. However, the actual picture is more subtle as the TAE 's do not emerge suddenly at the crossing. Instead, we find that there is a continuous transition from cascade-type modes to TAEs. The conventional TAE theory is insufficient to describe the transition because the shear is exactly zero at the crossing and the slope of the q-profile can no longer be treated as a constant at the mode location. A conceptually relevant approach to the case of very low shear was developed in Ref. [12], where it was pointed out that the radial mode width in this case is typically larger than the poloidal wavelength. Another important feature of the low shear case is the existence of multiple TAEs in the same gap. In what follows, we adapt the approach of Ref. [12] to address the transition from $q_0 > q_{TAE}$ to $q_0 < q_{TAE}$.

It is allowable to describe this transition in the framework of cold MHD since both the energetic particle and the plasma pressure effects become less significant than the toroidal coupling terms when the mode frequency reaches the TAE gap. The essence of the problem is captured by the following set of equations for the two coupled poloidal harmonics:

$$\frac{d}{dx} D_m \frac{d}{dx} \xi_m - D_m \xi_m + \frac{\varepsilon + \Gamma}{2} \xi_{m+1} + \frac{\varepsilon + 2\Gamma}{2} \xi_{m-1} + \frac{\varepsilon}{2} \xi_{m-1} = 0 \qquad (3)$$

$$\frac{d}{dx} D_{m-1} \frac{d}{dx} \xi_{m-1} - D_{m-1} \xi_{m-1} + \frac{\varepsilon + \Gamma}{2} \xi_m + \frac{\varepsilon + 2\Gamma}{2} \xi_m + \frac{\varepsilon}{2} \xi_m = 0, \qquad (4)$$

where $x = (r - r_0)m / r_0$ is the normalized radial coordinate, $\varepsilon = r_0 / R$ is the local aspect ratio, Γ is the Shafranov shift factor, and the quantities D_m and D_{m-1} are given by

$$D_m = \left[\varepsilon^2 \frac{q_0^2 R_0^2}{V_A^2} - (q_0 n - m)^2 - (q_0 n - m) \frac{r_0^2 q_0''}{q_0 m} x^2 \right]$$

$$D_{m-1} = \left[\varepsilon^2 \frac{q_0^2 R_0^2}{V_A^2} - (q_0 n - m + 1)^2 - (q_0 n - m + 1) \frac{r_0^2 q_0''}{q_0 m} x^2 \right].$$

For the radially extended modes with a mode width $\Delta x >> 1$, one can formally treat all the derivative terms in these equations as small compared to non-derivative terms. This approximation allows us to explicitly express ξ_{m-1} in terms of ξ_m and its derivatives and obtain a Schrödinger-type equation for ξ_m:

$$\frac{\square(\square+2\square\square)}{4}\square_{m}\square\square\square_{m}\left[\square 2\left|nq_0 - m+\frac{1}{2}\right|\left(q_0 n - m+\frac{1}{2}\square\frac{r_0^2 q_0''x^2}{q_0 m}+\left(\frac{r_0^2 q_0''x}{2q_0 m}\right)^2\right)+\frac{(\square+2\square\square)}{2}\frac{r_0^2 q_0''x}{q_0 m}\right] \quad (5)$$

$$=\square\square_{m}\left[\left(\frac{\square^2 q_0^2 R_0^2}{V_A^2}-(nq_0-m)^2\right)\left(\frac{\square^2 q_0^2 R_0^2}{V_A^2}-(nq_0-m+1)^2\right)\square\left(\frac{\square\square\square}{2}\right)^2\right]$$

We now observe that a change in q_0 from $q_0 > q_{TAE}$ to $q_0 < q_{TAE}$ changes the structure of the "potential energy" term from a single well to a double well, as shown in FIG. 2. The double-well case represents two preferred locations for TAEs on the opposite sides of the zero shear point. The single well case indicates that an eigenmode can exist even before q_0 crosses the value q_{TAE}. However, the long-wavelength approximation has a rather restrictive applicability condition in the single-well case. It requires $\square^2 m >> 4(q_0 n - m + 1/2)\frac{r_0^2 q_0''}{q_0}$, which is difficult to satisfy unless the mode is very close to the TAE gap or the q-profile is nearly flat, so that $r_0^2 q_0'' << q_0$. There are two effects that broaden the window of mode existence outside the TAE gap. The first one comes from the energetic particles with large orbits when these particles meet condition (2). This appears to be the main factor that gives rise to cascade modes in JET discharges with strongly reversed q-profiles.

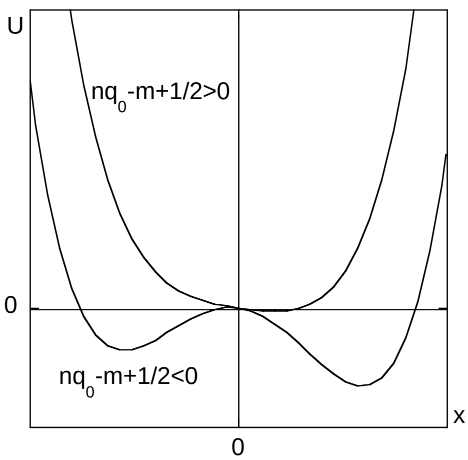

FIG. 2. Transformation of the effective potential for radially extended modes from a single well (nq_0-m+1/2>0) to a double well (nq_0-m+1/2<0).

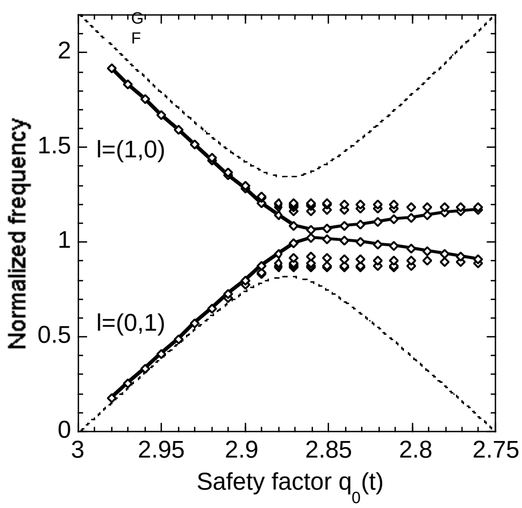

FIG. 3. Transition of Alfvén Cascade modes to TAE's. Diamonds present calculated eigenfrequencies for several radial modes with n=4 and m=(12;11).

The second effect comes from "diagonal" (in the poloidal mode number) $\square^2$-terms in the MHD operator for shear Alfvén waves. This is a geometric correction that arises from toroidicity but it is separate from the $\square^2$-terms included in Eq. (5) since it does not involve poloidal mode coupling. Our analysis shows that the geometric contribution changes condition (2) to

$$Q_{eff} = Q + m\square\frac{4q_0 R}{V_A}\frac{q_0}{r_0^2 q_0''}\square(\square+2\square\square) > 1/4 \quad (6)$$

The derivation of this result will be described elsewhere. Neither the energetic particle contribution nor the geometric correction changes the structure of Eqs. (3) and (4). They only

change the coefficients in the equations. Eqs. (3) and (4) with Q_{eff} included have been solved numerically to trace the transition from the nearly cylindrical long-wavelength cascade modes to TAEs as the safety factor q_0 changes in time. This reduced numerical model has been verified with the full geometry codes MISHKA [13] and CASTOR [14]. The long-wavelength approximation provides a relevant qualitative guidance for this numerical analysis.

Each calculated eigenmode can be labeled by its toroidal mode number *n*, a pair of poloidal mode numbers (assuming that the mode contains predominantly *m*-th and *(m-1)*-th poloial components), and a radial label *l*, which is the number of zeros (nodes) in the radial eigenfunctions for each of the *m*-th and *(m-1)*-th poloidal components respectively. FIG. 3 shows a set of eigenfrequencies for several radial modes with the same values of *n* and *m*. The two solid curves trace the frequencies of the modes with *l*=(0; 1) (lower curve) and *l*=(1; 0) (upper curve) as a function of q_0. The dotted curves in the figure mark the Alfvén continuum frequencies for the selected values of *n* and *m*. This figure demonstrates a strong asymmetry in the mode frequency behavior: the mode first stays close to the continuum frequency until q_0 reaches q_{TAE}. and then detaches from the continuum and moves into the TAE gap rather than tracking the continuum which would reverse the direction of frequency chirping.

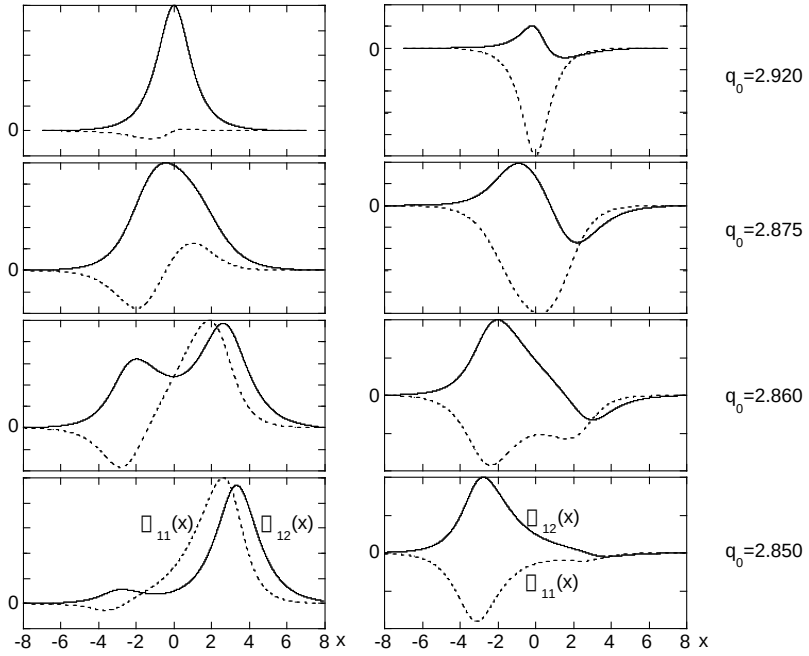

FIG. 4. Snapshots of the mode structure for n=4 and m=(12; 11) during the transition from a cascade mode to TAE. The left column shows the radial profiles of the m=12 and m=11 poloidal components for the lower [l=(0; 1)] mode of FIG. 3. The right column shows the upper mode [l=(1; 0)]. The values of q_0 for the snapshots are indicated next to the plots.

This pattern is consistent with the evolution of the potential well in Eq. (5), and the same general trend is clearly seen in the experimental data in FIG. 1. The calculated evolution of the mode structure along the solid curves of FIG. 3 provides additional evidence that the cascade modes indeed convert “adiabatically” into TAEs. FIG. 4 illustrates how the initial cylindrical cascade mode with a single dominant poloidal component ξ_{12} gains a second component due to toroidal coupling as the mode frequency approaches the TAE gap. Once in the gap, the mode then exhibits the typical signature of TAE, i.e. two nearly equal and strongly coupled poloidal components. Another characteristic feature in FIG. 4 is that the

mode acquires a double-hump structure when the effective "potential energy" in Eq. (5) changes from a single well to a double well. Later in its evolution the δ_{12} - component returns to a single hump structure that is now shifted from the zero shear point. The shift comes from an asymmetry of the double potential well, which forces the lower mode to concentrate predominantly in one of the two adjacent wells. The upper mode obviously "prefers" the other half of the well and it is therefore shifted to the left from the zero shear point. Also, the upper mode has an anti-ballooning poloidal structure in the TAE gap (the opposite signs of the poloidal components cause mode localization on the inner part of the torus) whereas the lower mode exhibits a ballooning structure (mode localization on the outer part of the torus). FIG. 1 shows that the upper modes are clearly present in the data, although they are typically not as intense or as frequent as the lower modes.

4. Alfvén Cascades as a Diagnostic Tool

Observations of Alfvén Cascades on JET have evolved into a valuable diagnostic tool [8, 9].

First, the very existence of ACs in the discharge indicates that the equilibrium has a reversed magnetic shear. Since the magnetic spectrograms can be processed very fast, on the inter-shot time scale, it is convenient to use ACs to monitor reversed shear regimes and to adjust parameters for subsequent discharges. A series of previously unexplored scenarios for obtaining shear-reversed equilibria was developed on JET with the aid of this type of AC diagnostic. This includes scenarios with NBI-only and on-axis ICRH pre-heating schemes, as well as scenarios with pellet injection.

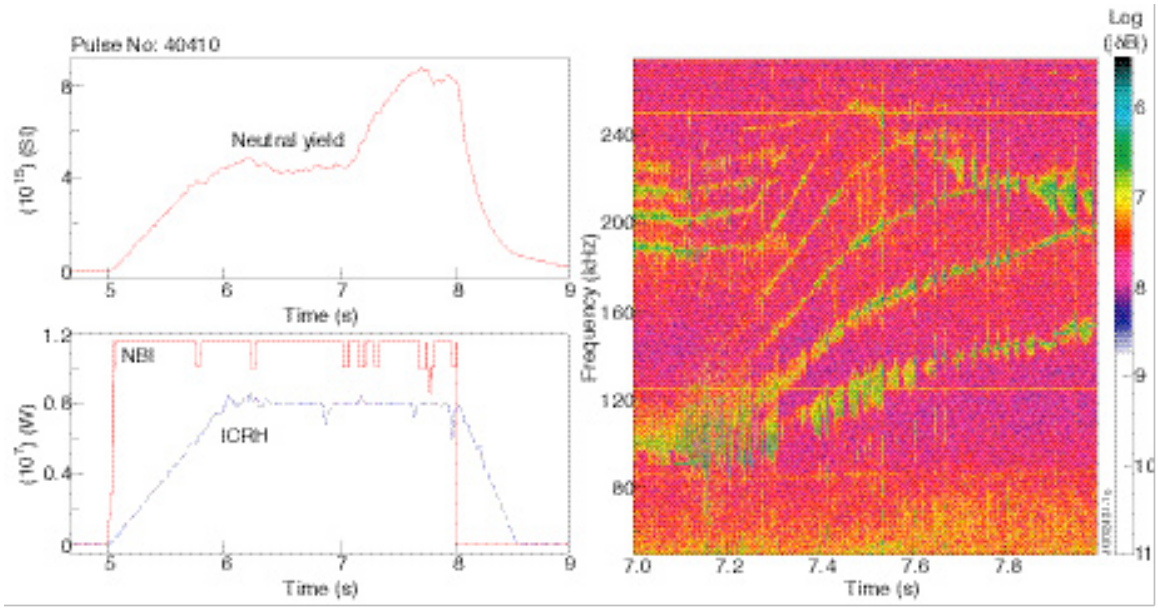

FIG. 5a. Temporal evolution of the neutron rate, $R_{NT}(sec^{-1})$, P_{NBI} (W) and P_{ICRF} (W) in discharge #40410.

FIG. 5b. Spectrogram of the magnetic perturbations, δB_p, measured by the external Mirnov coils in discharge #40410.

Second, it follows from Eq. (1) that the cascade modes with different mode numbers satisfy the condition $m - nq_{\min}(t) = 0$ at different times as $q_{\min}(t)$ passes rational magnetic surfaces. For example, the $n = 1$ rational surfaces occur when $q_{\min}$ passes integer values 1, 2, 3…; the $n = 2$ rational surfaces occur when $q_{\min}$ passes integer and half-integer values 1, 3/2, 2,

5/2…; $n = 3$ rational surfaces occur when $q_{\min}$ passes 1, 1.33, 1.67, 2, 2.33…etc. Applying this observation to the pattern of cascades, one can learn how the $q_{\min}$ value is evolving in time [9]. Typically such estimates compare rather well with MSE measurements, which makes them a useful corroborative crosscheck. It should also be noted that the cascade diagnostic uses ICRH produced ions, as opposed to neutral beams needed for MSE.

Third, it was found on JET that multiple Alfven Cascade modes with several different toroidal mode numbers emerge simultaneously with Internal Transport Barrier (ITB) triggering events. These events give rise to ITB formation provided that there is sufficient power input [15]. FIGs. 5a and 5b demonstrate the correlation between an AC and a sudden increase in the neutron yield, caused by an ITB formation in a stationary plasma with stationary heating. The toroidal magnetic field in the pulse of interest was 3.4 T, the plasma current 3 MA. The main heating phase of the discharge had 8 MW of ICRF and 12 MW of NBI power. In addition, 1÷2 MW of LHCD was applied at the pre-heating phase. The current flat-top started at t = 6.8 sec. FIG. 5a shows that the neutron rate, which was quasi-stationary for a very long time, increases suddenly by a factor of two at t = 7.1 sec at a constant power of NBI and ICRH. The spectrum of MHD events during the same time interval (FIG. 5b) reveals a set of AC modes with upward frequency chirping that starts at t = 7 sec, simultaneously with the ITB formation and the increase in neutron yield. The correlation between the multiple ACs and the ITB triggering is consistent with the notion that both events are associated with an integer value of $q_{\min}$. For the case presented in FIGs. 5a and 5b, we conclude that $q_{\min}$ =2 at the cascade onset that occurs at t = 7sec.

References

[1] WONG, K.L., et al., Phys. Rev. Lett. **66** (1991) 1874.
[2] ITER Physics Expert Group on Energetic Particles, Heating and Current Drive, ITER Physics Basis Editors, Nucl. Fusion **39** (1999) 2471.
[3] GOELDBLOED, J.P., et al., Plasma Physics Controlled Fusion **35** (1993) B277.
FASOLI, A., et al., “MHD Spectroscopy”, to be published in Plasma Physics Controlled Fusion (2002).
[4] CHENG, C.Z., CHEN, L., CHANCE, M.S., Ann. Phys.**161** (1985) 21.
CHENG, C.Z. and CHANCE, M.S., Phys. Fluids **29** (1986) 3659.
[5] ROSS, D.W., CHEN, G.L. and MAHAJAN, S.M., Phys. Fluids **25** (1982) 652.
[6] APPERT, K., et al., Plasma Phys. Control Fusion **24** (1982) 1147 .
[7] KIMURA, H., et al., Nucl. Fusion **38** (1998) 1303.
[8] SHARAPOV, S.E., et al., Phys. Lett. A **289** (2001) 127.
[9] SHARAPOV, S.E., et al., Phys. Plasmas **9** (2002) 2027.
[10] BERK, H.L., et al., Phys. Rev. Lett. **87** (2001) 185002.
[11] BERK, H.L., BREIZMAN, B.N. and PEKKER, M.S., Plasma Phys. Rep. **23** (1997) 778.
[12] CANDY, J., et al., Phys. Lett. A **215** (1996) 299.
[13] HUYSMANS, G.T.A., et al., Phys. Plasmas **8** (2001) 10.
[14] KERNER, W., et al., J. Comp. Phys. **142** (1998) 271.
[15] JOFFRIN, E., et al., Plasma Phys. Control Fusion, **44** (2002) 1739.